Hindawi
International Journal of Polymer Science
Volume 2017, Article ID 7594950, 7 pages
https://doi.org/10.1155/2017/7594950

Research Article

Molecular Dynamics Simulation to Understand the Ability of Anionic Polymers to Alter the Morphology of Calcite

Insil Choi and Il Won Kim

Department of Chemical Engineering, Soongsil University, Seoul 06978, Republic of Korea

Correspondence should be addressed to Il Won Kim; iwkim@ssu.ac.kr

Received 29 March 2017; Accepted 11 June 2017; Published 17 July 2017

Academic Editor: Bernabé L. Rivas

Molecular dynamics was utilized to investigate the ability of anionic macromolecules to drastically change the morphology of calcite in the presence of magnesium ions. Anionic poly(acrylic acid) and poly(methacrylic acid) were compared with cationic poly(ethylene imine) in their binding behavior on calcite (104) and (110) surfaces. Poly(acrylic acid) and poly(methacrylic acid) showed preferential binding on (110) with strong electrostatic attractions, whereas poly(ethylene imine) was only weakly attracted to (104). The extent of the charge imbalance on the surfaces appeared responsible for the current results, which originated from the deficient number of the coordinating oxygen atoms of carbonate around the surface calcium. The results of the current study were in accordance with the previous experimental observations, where the {hk0} surfaces of calcite were elongated under the coexistence of the anionic polymers and magnesium ions. These results could be generally utilized in the polymer-controlled crystallization with broad implications in the specific interactions with crystal surfaces.

1. Introduction

Biominerals have been studied as unusual model systems of crystallization because of their exquisite structural characteristics [1]. Particularly, calcium carbonate-based biominerals have provided interesting examples of the crystals with highly controlled polymorphs and morphologies [2, 3]. Both the polymorphic selection and morphological control have been attributed to the organic macromolecules acting on the inorganic crystallization [2–4]. While the full details of the macromolecular controls are to be revealed upon the more extensive future examinations, one of the most important features appears to be the specific interactions between the macromolecules and the crystals of calcium carbonate.

Magnesium is also another contributory factor, which has been recognized as being important in the formation of amorphous precursor as well as the morphology control of calcium carbonate [1, 3, 5–8]. In addition, the cooperative effects of the biomacromolecules and the magnesium ions were found in the case of Asprich proteins from *Atrina rigida* [9, 10]. The coexistence of the acidic proteins and magnesium dramatically changed the morphology of the calcite polymorph of calcium carbonate to create crystals exposing predominantly {hk0} faces, whereas {104} was dominant without either one of the components (Figure 1). This behavior was also mimicked through the use of synthetic polymers rich in carboxylic acids, confirming the cooperative effects [11].

In the present study, the mechanism of the modification of calcite morphology by the acidic macromolecules was further explored with the aid of molecular dynamics. The previous molecular model was based on the different oxygen-coordinating numbers around calcium ions on different calcite surfaces (thermodynamically stable {104} and magnesium-stabilizing {hk0}) [10, 11]. While this model appeared qualitatively reasonable to explain the varying degree of the macromolecular interactions, it could be too simplistic not considering the dynamic nature of mineral surfaces in the presence of water molecules. On the other hand, approaches using molecular dynamics have been successfully utilized to explain the interactions of various organic molecules on the calcite surfaces [12–16]. Similarly, the present molecular dynamics study could generate a more realistic model to clarify the mechanism of the cooperative

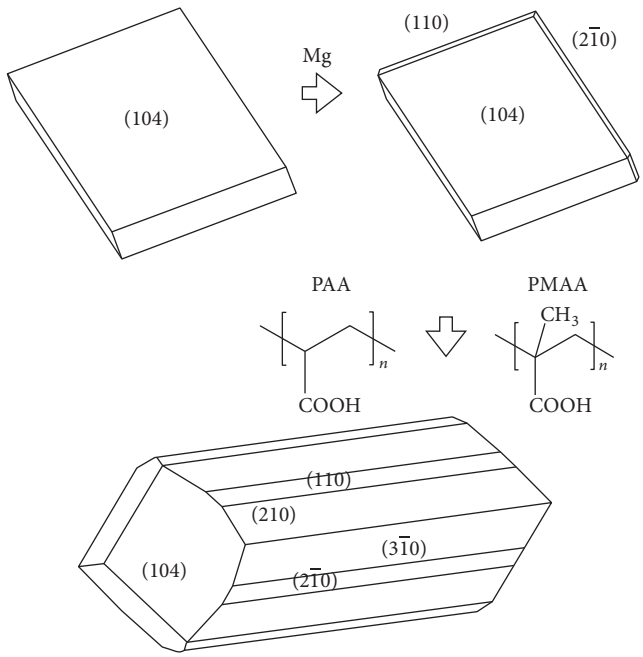

Figure 1: Schematic description of the morphological variation of calcite with the cooperative effects of anionic polymers and Mg(II).

effects. This might in turn provide interesting implications useful in the field of polymer-induced crystallization [17–19].

2. Methods

The generation of the calcite surfaces was based on the known crystallographic structure [20]. Forcite Plus module of Materials Studio software (2016, BIOVIA, San Diego, CA, USA) was utilized to import and optimize the structure through energy minimization under COMPAS II force field [21, 22]. The optimized calcite structures were cleaved to expose either (104) or (110) surfaces. The thickness normal to the surfaces was set to have four layers of calcium carbonate parallel to the cleaved surfaces. The top two layers of the surfaces were then relaxed during geometrical optimization. Finally, three-dimensional simulation boxes were constructed from the surfaces to be able to contain water and the polymer molecules. The sizes of the boxes were $81 \times 100 \times 65$ Å^3 and $81 \times 102 \times 65$ Å^3 for (104) and (110), respectively.

The aqueous solutions of polymers to be set in contact with calcite surfaces were constructed in three steps. Firstly, polymer molecules with ionized functional groups were formed according to the chosen experimental conditions (molecular weights of polymers and pH) in the previous study [11]. The number of repeating units of poly(acrylic acid) (PAA), poly(methacrylic acid) (PMAA), and poly(ethylene imine) (PEI) was 25, 25, and 30, respectively. After structural optimization in the same way for the calcite, 20 carboxylic acids and 3 primary amines were ionized according to the ionization degrees at pH 8: 0.8 for PAA and PMAA and 0.1 for PEI [23–25]. Specific functional groups in the polymer chains to be ionized were selected through random number generation using the RANDBETWEEN function of Microsoft Excel software. Secondly, the ionized polymer molecules were placed in the simulation boxes. They were located at the center of each surface and at least 5 Å afloat from the surface. Calcium and chloride were selected as counterions to create neutral systems (total charge of zero), which were located at least 20 Å away from the polymers. Finally, the simulation boxes were packed with water molecules with a density of 1 g/cm^3 using the Amorphous Cell module of Materials Studio.

The molecular dynamics was performed in NVT (constant number, volume, and temperature) ensemble at 288 K using Nosé thermostat to follow the experimental temperature in the previous study [11, 26]. The systems were equilibrated for 100 ps with a time step of 1 fs under COMPASS II force field, and the charges assigned in the force field were adopted [27]. Ewald and atom-based summations were applied for Coulomb and van der Waals interactions, respectively [28].

Binding energies of the polymers to the calcite surfaces, E(binding), were calculated as E(binding) = E(calcite-polymer-water) − E(calcite-water) − E(polymer-water) − E(calcite) − E(polymer) − E(water), where E(calcite-polymer-water) is the total energy, E(calcite-water) is the interaction energy between calcite and water, and E(polymer-water) is the interaction energy between polymer and water. E(calcite), E(polymer), and E(water) are the energies of free calcite, polymer, and water, respectively. The reported average values of the binding energies were from the three final structures.

3. Results and Discussion

Calcite (104) and (110) surfaces were selected to compare the binding behaviors of PAA (25-mer), PMAA (25-mer), and PEI (30-mer). The (104) is the typical face observed in the well-shaped crystals of calcite [29, 30]. The (110) is used to represent {hk0} faces [10, 12, 14]. In calcite, one calcium is surrounded by six oxygen atoms from carbonate. The spatial atomic arrangement of calcite is such that the calcium on the (104) surface is encircled by five oxygen atoms while that on the (110) only by four [20]. The less favorable nature of the (110) to become an exposed surface was also pointed out in the periodic bond chain model of Hartman and Perdok, where the (110) was classified as less strong F (flat) or S (stepped); (104) displayed the strongest F [31]. (The lack of oxygen is similar for other simple {hk0} surfaces; e.g., calcium on K (kinked) (120) and S (100) surfaces was surrounded by four and three oxygen atoms, resp.) Figure 2 shows the structure of calcite (104) and (110) surfaces stabilized in the presence of water under the molecular dynamics conditions utilized in this study. The (110) surface underwent severer modification than (104) (Figures 2(a) and 2(b)), which was expected from the less charge-balanced state as previously described. This is also in accordance with the more disrupted nature of the (110) surface found in the previous studies [12, 14]. Particularly, the disruption is notable with the disorganized carbonate molecules and the penetration of water molecules into the outer layer of calcite (110). The concentration profiles for the atoms in calcite and water (Figures 2(c) and 2(d)) distinctly

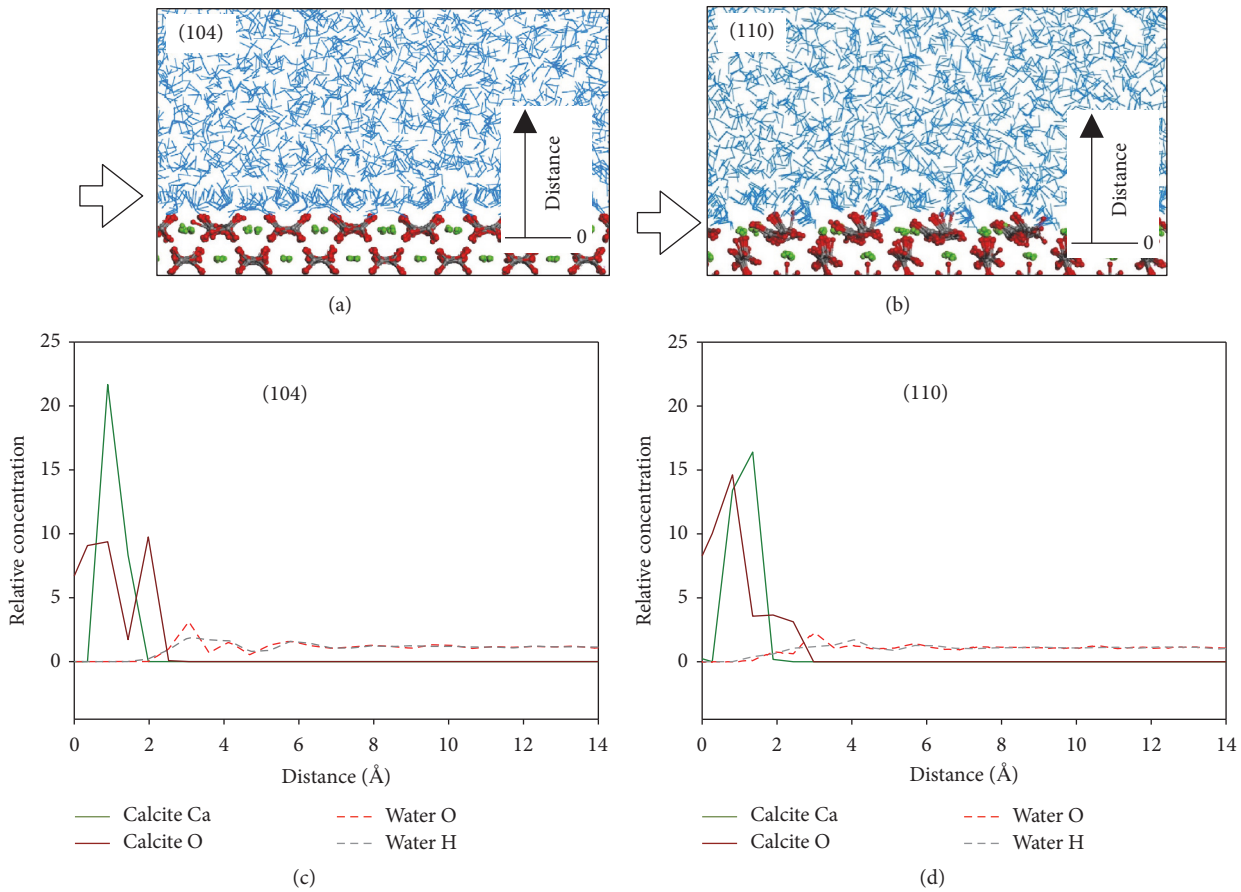

Figure 2: Representative structures of calcite surfaces stabilized in the presence of water: (a) (104); (b) (110). Concentration profiles of atoms in calcite and water are displayed for (c) (104) and (d) (110) systems.

Table 1: Binding energies (kcal/mol) of PAA, PMAA, and PEI on the calcite surfaces.

Surface	PAA	PMAA	PEI
(104)	−244.6 ± 87.6	−399.3 ± 17.4	−22.8 ± 7.9
(110)	−471.0 ± 29.7	−521.9 ± 100.1	33.8 ± 2.1

show the relatively low carbonate concentration and the water penetration on (110) and well-structured carbonate and adjacent water layers on (104) (see the arrows in Figures 2(a) and 2(b)) [14].

Binding energies of PAA, PMAA, and PEI on calcite (104) and (110) surfaces were summarized in Table 1. PAA and PMAA preferred the (110) over the (104) surface for their binding. The differences of the binding energies between the studied surfaces were ca. 226 and 123 kcal/mol for PAA and PMAA, respectively. The differences were quite large compared to the thermal energy (RT) of 0.57 kcal/mol at the simulation temperature of 288 K. In addition, the individual binding energy on (104) (ca. −245 and −399 kcal/mol for PAA and PMAA, resp.) was in the same order as that of the (104) attachment energy (ca. −367 kcal/mol) calculated by the growth morphology task (Morphology module in Materials Studio) using the same force field COMPASS II. This is in accordance with the experimental observation of PAA and PMAA frustrating the normal growth of calcite to form staircase-like crystal morphologies [11]. (We note here that the similar studies reported a diverse range of binding energies for several carboxylic acid-containing adsorbates probably because of the various stages of energy minima found in the particular studies [13, 15, 16]; e.g., simple tartrate showed preferred adsorption on (1–10) (−9.1 kcal/mol) over (104) (−1.6 kcal/mol), and nonanoic acid with one carboxylic acid showed interaction energy of −40 kcal/mol with (110) [13, 16].) In contrast, PEI showed weak preferential binding on (104) (ca. −23 kcal/mol), and its binding on (110) was unstable with a positive value of binding energy. In addition, its binding energy on (104) was much less than the attachment energy of (104), which was also in accordance with the experimental observation of PEI not affecting the general rhombohedral morphology of calcite [11]. Overall, the calculated binding energies clearly showed that the negatively charged PAA and PMAA preferred the (110) surface of calcite over (104), which could explain their ability to elongate the {hk0} surfaces during crystal growth with the aid of Mg(II) initially stabilizing a small area of the {hk0} [10, 32].

The representative conformations of PAA, PMAA, and PEI on calcite (104) and calcite (110) are shown in Figure 3. The overall conformations of the polymers were subtly

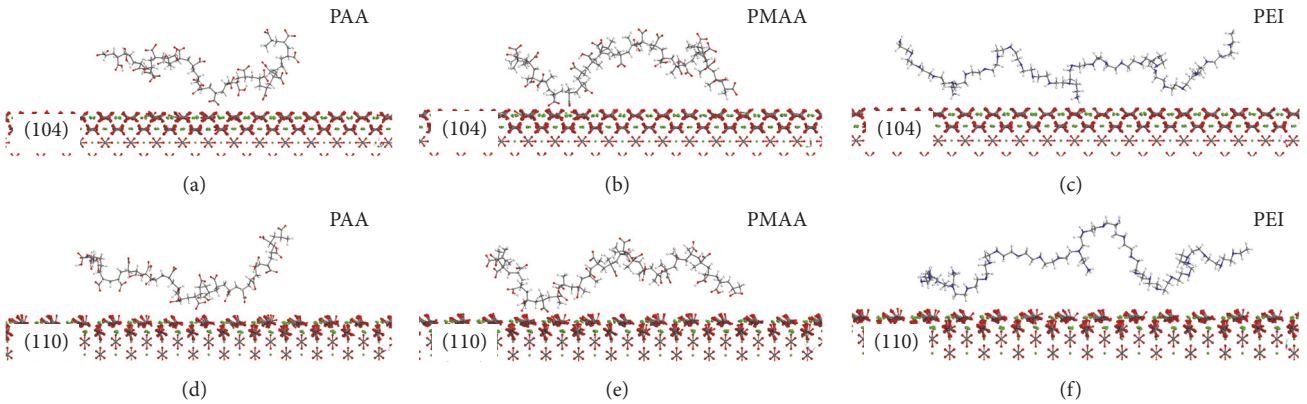

Figure 3: Representative binding conformations of polymer molecules on calcite: (a) PAA on (104); (b) PMAA on (104); (c) PEI on (104); (d) PAA on (110); (e) PMAA on (110); (f) PEI on (110). Calcium, oxygen, nitrogen, carbon, and hydrogen atoms are portrayed in green, red, blue, grey, and white, respectively. Water molecules are not shown for clarity.

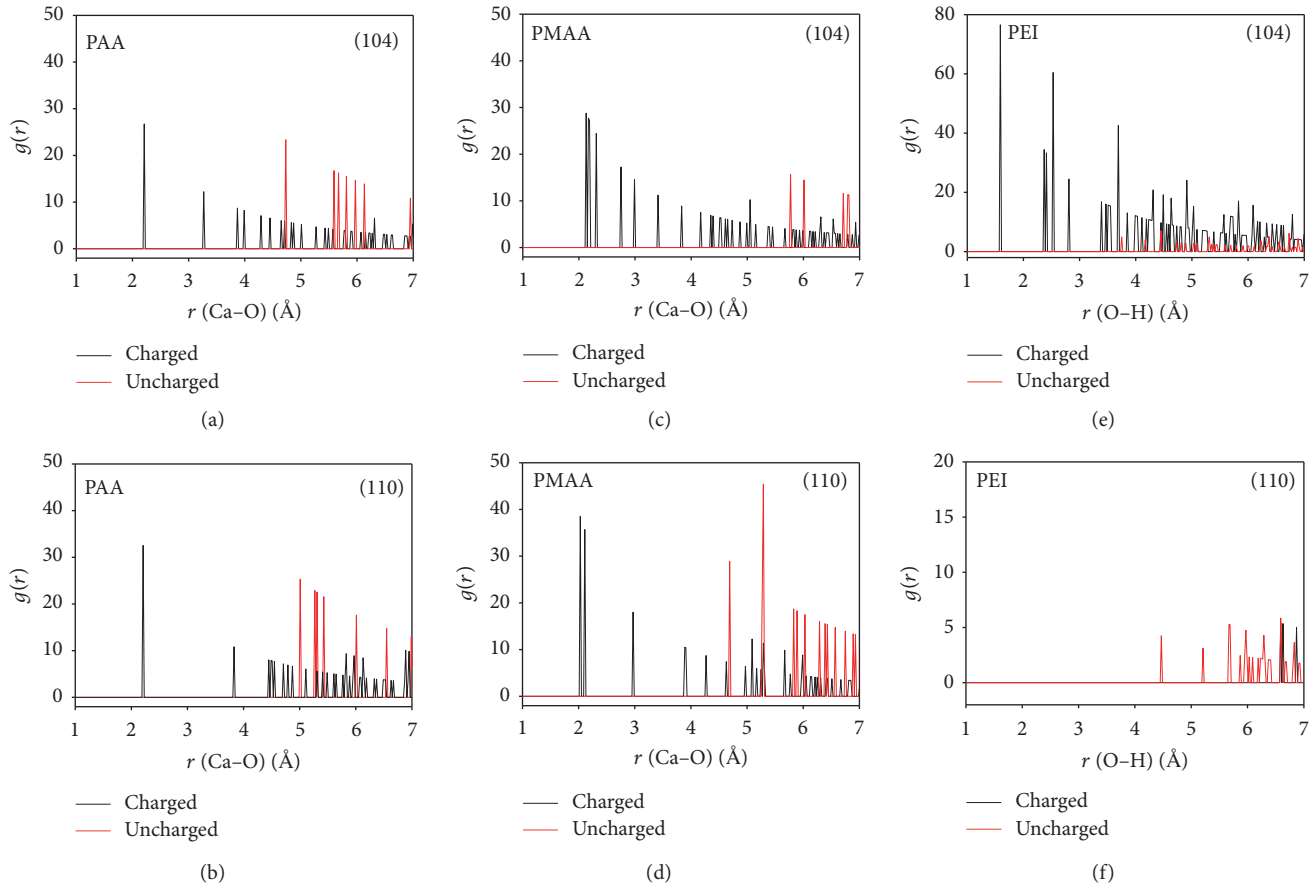

Figure 4: Pair distribution functions of Ca (calcite)–O (carboxyl) for PAA on (104) (a) and (110) (b); PMAA on (104) (c) and (110) (d). Pair distribution functions of O (calcite)–H (amino) for PEI on (104) (e) and (110) (f).

affected by the calcite surfaces, and the level of the influence was greater for PAA and PMAA than PEI. The end-to-end distances were 52.3 Å (before interacting with calcite), 36.8 ± 0.4 Å (after binding on 104), and 39.4 ± 1.7 Å (after binding on 110) for PAA; 48.0 Å (before), 39.1 ± 0.1 Å (on 104), and 43.1 ± 1.1 Å (on 110) for PMAA; 60.8 Å (before), 61.6 ± 0.4 Å (104), and 60.1 ± 0.2 Å (110) for PEI. The values after binding were formed from the average of three final structures.

Analysis of the spatial profiles of the polymers bound on calcite surfaces showed the distinct difference between PAA/PMAA and PEI. Figure 4 displays the pair correlation functions that quantify the spatial relationships. For the

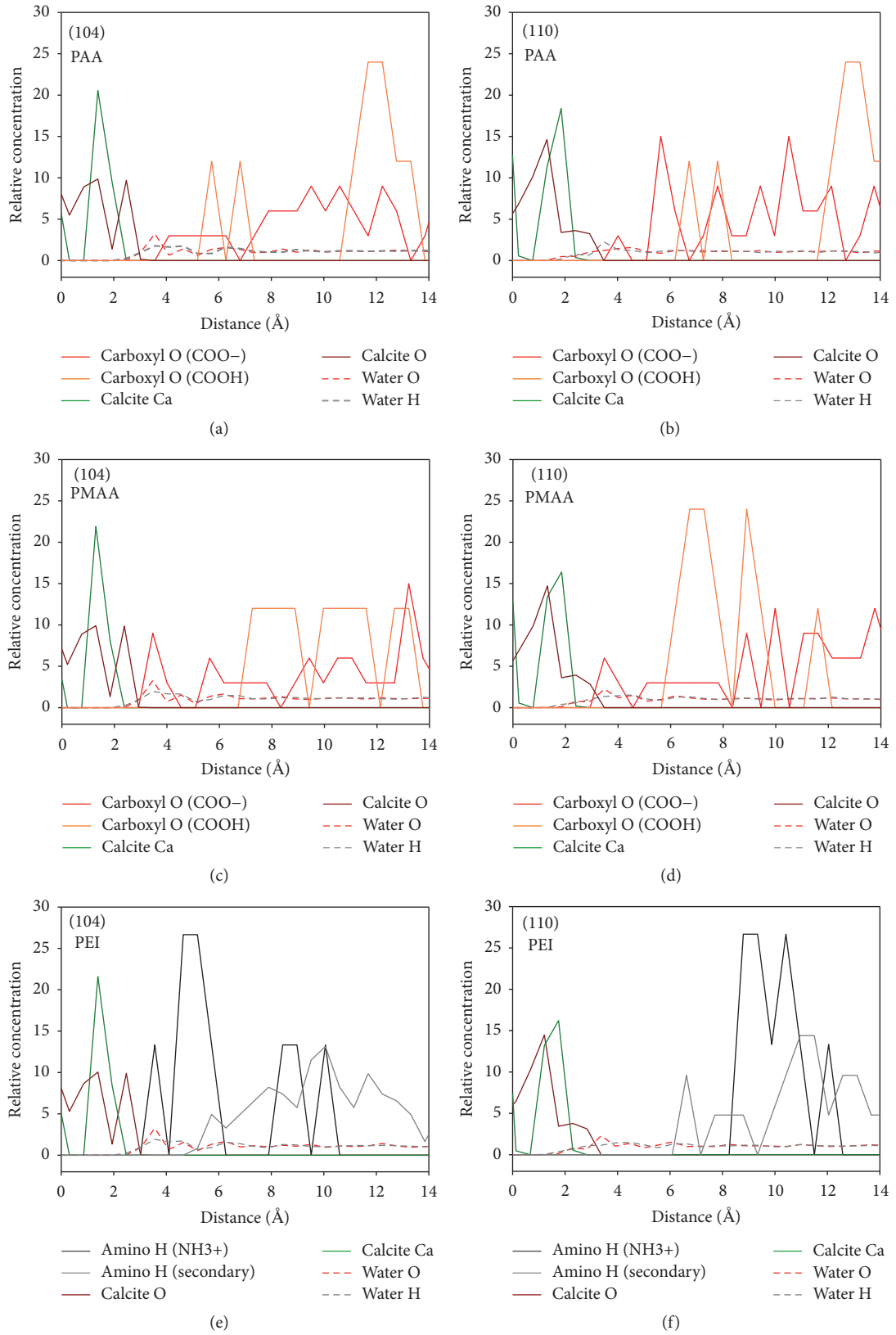

Figure 5: Concentration profiles of various atoms in calcite, water, and polymers in the (104) and (110) systems.

negatively charged PAA and PMAA, the pair correlation functions show the distance between the calcium in the top layer of calcite and the oxygen of the carboxylic groups of the polymers. For the positively charged PEI, it is between the surface oxygen atoms of calcite and the hydrogen atoms of the amine groups of the polymer. The shortest distances are 2.21 Å (110) and 2.21 Å (104) for PAA with a slightly higher intensity at (110); 2.03 (additionally 2.11) Å (110) and 2.13 Å (104) for PMAA; 6.59 Å (110) and 1.59 Å (104) for PEI. To the (104) surfaces, the charged carboxylic acid groups of PAA and PMAA as well as the charged primary amine groups of PEI were attracted. However, to the (110), the charged carboxylic acids of PAA/PMAA were attracted, and the charged primary amines of PEI were relatively repelled. Again, this is in a good agreement with the experimentally observed {hk0} enlargement in the presence of PAA and PMAA. No such effect was observed with PEI.

Figure 5 provides more comprehensive information on the spatial distributions of atoms involved in the current study. As stated with Figure 2, the (110) surfaces possessed the more disrupted top layers than (104), which originated from the fact that the calcium on (110) was more deficiently surrounded by the oxygen atoms from carbonate: four oxygen atoms at (110) versus five at (104). The deficiently surrounded calcium on (110) apparently contributed to the high binding energies of the negatively charged PAA and PMAA (Figures 5(a)–5(d)). Also, the repulsive interactions with carbonate appeared less severe on (110), since the relative concentration of carbonate on (110) was intrinsically low, and the water molecules penetrating into the less organized top layers appeared to suppress the repulsive contribution further (Figures 5(b) and 5(d)) [14, 16]. The situation was reversed for the positively charged PEI. While PEI was weakly attracted to the (104) surface with well-organized carbonate and adjacent water layers, it experienced dominant electrostatic repulsion by calcium on (110) (Figures 5(e) and 5(f)). The binding of the PAA and PMAA on both (110) and (104) was mostly of electrostatic nature (>95% of the total binding energy). When PEI was weakly attracted to the (104) surface the electrostatic contribution was about 46% of the binding energy, the rest being the van der Waals interactions. Overall, the atomic concentration profiles combined with the binding energy analysis clarified the nature of the strong binding of the PAA and PMAA on calcite (110).

We note that anionic polymers including PAA have been extensively studied as scale inhibitors as well as particle stabilizers when calcite was the inorganic phase [33–37]. In both cases, the polymeric adsorption on calcite was one of the key processes, and it was often accompanied by the subtle morphological changes of calcite. Therefore, the results of the current study might be also useful in designing the optimal scale inhibitors or particle stabilizers.

4. Conclusions

In summary, the mechanism of morphology modification observed in the biomimetic and bioinspired mineralization of calcite was studied using molecular dynamics simulation. The previous experimental study showed the ability of PAA and PMAA to form the staircase-like morphology of calcite surrounded by {104} faces when acting alone and generate the extended morphology largely covered by new {hk0} faces when Mg(II) coexisted [11]. The current study showed that the binding energies of PAA and PMAA to (104) were comparable to the attachment energy of (104), and more importantly they preferred to bind Mg(II)-stabilized (110) over the typical (104). The involved binding energies of PAA and PMAA were mostly of the electrostatic nature, which confirmed the importance of the charge imbalance on the specific surface of calcite. In essence, the current study reinforced the previous simple molecular model by providing more quantitative information on the preferential binding of the macromolecules. Further study would be necessary to search for other pairs of molecules exhibiting similar combined effects. Eventually, such cooperative effects, if established as general approaches, could expand the utility of the polymeric additives in the control of crystal growth morphology [17–19].

Conflicts of Interest

The authors declare that there are no conflicts of interest regarding the publication of this paper.

Acknowledgments

This research was supported by the Basic Science Research Program through the National Research Foundation of Korea (NRF) funded by the Ministry of Education (NRF-2015R1D1A1A01058116).

References

[1] H. A. Lowenstam and S. Weiner, *On Biomineralization*, Oxford University Press, New York, NY, USA, 1989.

[2] A. M. Belcher, X. H. Wu, R. J. Christensen, P. K. Hansma, G. D. Stucky, and D. E. Morse, "Control of crystal phase switching and orientation by soluble mollusc-shell proteins," *Nature*, vol. 381, no. 6577, pp. 56–58, 1996.

[3] S. Weiner and L. Addadi, "Design strategies in mineralized biological materials," *Journal of Materials Chemistry*, vol. 7, no. 5, pp. 689–702, 1997.

[4] L. Addadi, D. Joester, F. Nudelman, and S. Weiner, "Mollusk shell formation: a source of new concepts for understanding biomineralization processes," *Chemistry—A European Journal*, vol. 12, no. 4, pp. 980–987, 2006.

[5] F. Lippmann, *Sedimentary Carbonate Minerals*, Springer Berlin Heidelberg, Berlin, Germany, 1973.

[6] S. Raz, P. C. Hamilton, F. H. Wilt, S. Weiner, and L. Addadi, "The transient phase of amorphous calcium carbonate in sea urchin larval spicules: the involvement of proteins and magnesium ions in its formation and stabilization," *Advanced Functional Materials*, vol. 13, no. 6, pp. 480–486, 2003.

[7] J. M. Kanold, M.-L. Lemloh, P. Schwendt et al., "In vivo enrichment of magnesium ions modifes sea urchin spicule properties," *Bioinspired, Biomimetic and Nanobiomaterials*, vol. 4, no. 2, pp. 111–120, 2015.

[8] M. Sancho-Tomás, S. Fermani, M. Reggi, J. M. García-Ruiz, J. Gómez-Morales, and G. Falini, "Polypeptide effect on Mg2+

hydration inferred from CaCO3 formation: A biomineralization study by counter-diffusion," *CrystEngComm*, vol. 18, no. 18, pp. 3265–3272, 2016.

[9] B.-A. Gotliv, N. Kessler, J. L. Sumerel et al., "Asprich: a novel aspartic acid-rich protein family from the prismatic shell matrix of the bivalve Atrina rigida," *ChemBioChem*, vol. 6, no. 2, pp. 304–314, 2005.

[10] I. W. Kim, S. Collino, and J. S. Evans, "Cooperative modulation of mineral growth by prismatic-associated Asprich sequences and Mg(II)," *International Journal of Molecular Sciences*, vol. 13, no. 3, pp. 3949–3958, 2012.

[11] T. Yang, D. Kim, E. Huh, J. Y. Jho, and I. W. Kim, "Regulating the morphology of calcite through selective binding of polymers with carboxylic acids," *Polymer (Korea)*, vol. 40, no. 5, pp. 813–817, 2016.

[12] N. H. De Leeuw and S. C. Parker, "Atomistic simulation of the effect of molecular adsorption of water on the surface structure and energies of calcite surfaces," *Journal of the Chemical Society - Faraday Transactions*, vol. 93, no. 3, pp. 467–475, 1997.

[13] B. Rai and Pradip, "Rational design of selective industrial performance chemicals based on molecular modeling computations," in *Molecular Modeling for the Design of Novel Performance Chemicals and Materials*, B. Rai, Ed., pp. 27–64, CRC Press, Boca Raton, Fla, USA, chapter 2 edition, 2012.

[14] H. Nada, "Difference in the conformation and dynamics of aspartic acid on the flat regions, step edges, and kinks of a calcite surface: a molecular dynamics study," *Journal of Physical Chemistry C*, vol. 118, no. 26, pp. 14335–14345, 2014.

[15] D. J. Sparks, M. E. Romero-González, E. El-Taboni et al., "Adsorption of poly acrylic acid onto the surface of calcite: an experimental and simulation study," *Physical Chemistry Chemical Physics*, vol. 17, no. 41, pp. 27357–27365, 2015.

[16] M. Ukrainczyk, M. Greiner, E. Elts, and H. Briesen, "Simulating preferential sorption of tartrate on prismatic calcite surfaces," *CrystEngComm*, vol. 17, no. 1, pp. 149–159, 2015.

[17] S. Jung, J.-M. Ha, and I. W. Kim, "Phase transformation of adefovir dipivoxil/succinic acid cocrystals regulated by polymeric additives," *Polymers*, vol. 6, no. 1, pp. 1–11, 2014.

[18] L. Y. Pfund and A. J. Matzger, "Towards exhaustive and automated high-throughput screening for crystalline polymorphs," *ACS Combinatorial Science*, vol. 16, no. 7, pp. 309–313, 2014.

[19] J. H. Choi, Y. G. Hong, S. Lee, and J. W. Lee, "Determination of polymer content in polymer bonded explosives and their simulants," *Polymer Korea*, vol. 41, no. 1, pp. 53–60, 2017.

[20] D. L. Graf, "Crystallographic tables for the rhombohedral carbonates," *American Mineralogist*, vol. 46, no. 11-12, pp. 1283–1316, 1961.

[21] H. Sun, "Compass: an ab initio force-field optimized for condensed-phase applications—overview with details on alkane and benzene compounds," *Journal of Physical Chemistry B*, vol. 102, no. 38, pp. 7338–7364, 1998.

[22] H. Sun, Z. Jin, C. Yang et al., "COMPASS II: extended coverage for polymer and drug-like molecule databases," *Journal of Molecular Modeling*, vol. 22, no. 2, article 47, pp. 1–10, 2016.

[23] A. Laguecir, S. Ulrich, J. Labille, N. Fatin-Rouge, S. Stoll, and J. Buffle, "Size and pH effect on electrical and conformational behavior of poly(acrylic acid): Simulation and experiment," *European Polymer Journal*, vol. 42, no. 5, pp. 1135–1144, 2006.

[24] R. Dong, M. Lindau, and C. K. Ober, "Dissociation behavior of weak polyelectrolyte brushes on a planar surface," *Langmuir*, vol. 25, no. 8, pp. 4774–4779, 2009.

[25] T. Yang, W. Huh, H. Kong, J. Y. Jho, and I. W. Kim, "Effects of polymer architecture and charge density on the pH-responsive Ca(II) release from brushite," *Colloids and Surfaces A: Physicochemical and Engineering Aspects*, vol. 459, pp. 74–81, 2014.

[26] S. Nosé, "A unified formulation of the constant temperature molecular dynamics methods," *The Journal of Chemical Physics*, vol. 81, no. 1, pp. 511–519, 1984.

[27] M. Svärd and Å. C. Rasmuson, "Force fields and point charges for crystal structure modeling," *Industrial and Engineering Chemistry Research*, vol. 48, no. 6, pp. 2899–2912, 2009.

[28] P. P. Ewald, "Evaluation of optical and electrostatic lattice potentials," *Annals of physics*, vol. 64, pp. 256–287, 1921.

[29] Y.-J. Han, L. M. Wysocki, M. S. Thanawala, T. Siegrist, and J. Aizenberg, "Template-dependent morphogenesis of oriented calcite crystals in the presence of magnesium ions," *Angewandte Chemie International Edition*, vol. 44, no. 16, pp. 2386–2390, 2005.

[30] I. W. Kim, J. L. Giocondi, C. Orme, S. Collino, and J. S. Evans, "Morphological and kinetic transformation of calcite crystal growth by prismatic-associated asprich sequences," *Crystal Growth and Design*, vol. 8, no. 4, pp. 1154–1160, 2008.

[31] P. Hartman and W. G. Perdok, "On the relations between structure and morphology of crystals. I," *Acta Crystallographica*, vol. 8, no. 1, pp. 49–52, 1955.

[32] K. J. Davis, P. M. Dove, L. E. Wasylenki, and J. J. De Yoreo, "Morphological consequences of differential Mg2+ incorporation at structurally distinct steps on calcite," *American Mineralogist*, vol. 89, no. 5-6, pp. 714–720, 2004.

[33] M. M. Reddy and A. R. Hoch, "Calcite crystal growth rate inhibition by polycarboxylic acids," *Journal of Colloid and Interface Science*, vol. 235, no. 2, pp. 365–370, 2001.

[34] Y. Tang, W. Yang, X. Yin, Y. Liu, P. Yin, and J. Wang, "Investigation of CaCO3 scale inhibition by PAA, ATMP and PAPEMP," *Desalination*, vol. 228, no. 1-3, pp. 55–60, 2008.

[35] R. Ketrane, B. Saidani, O. Gil, L. Leleyter, and F. Baraud, "Efficiency of five scale inhibitors on calcium carbonate precipitation from hard water: Effect of temperature and concentration," *Desalination*, vol. 249, no. 3, pp. 1397–1404, 2009.

[36] F. Garcia, N. Le Bolay, and C. Frances, "Rheological behaviour and related granulometric properties of dense aggregated suspensions during an ultrafine comminution process," *Powder Technology*, vol. 130, no. 1-3, pp. 407–414, 2003.

[37] B. Cheng, M. Lei, J. Yu, and X. Zhao, "Preparation of monodispersed cubic calcium carbonate particles via precipitation reaction," *Materials Letters*, vol. 58, no. 10, pp. 1565–1570, 2004.